Electronic Supplementary Information

The Role of Anionic Design in Modulating Material Properties: from SHG Switching to Ferroelastic Switching

Jia-Zi She, Yun-Hui Yu, Yan-Ran Weng, Dan Lu, Yong Yu, Ying Zhou, Hui-Peng Lv, and Yong Ai*

Corresponding author: yong.ai@ncu.edu.cn

Materials

Tetramethylammonium Hydroxide Pentahydrate, Methanesulfonic acid, and trifluoromethanesulfonic acid were purchased from Aladdin and without further purifying. Methyl alcohol and acetonitrile were purchased from Merck and used as the solvent.

Crystal Growth

Crystal of $[NMe_4][CH_3SO_3H]$ ($CH\text{-}NMe_4$) is grown by dissolving 18.1 g (100 mmol) of tetramethylammonium hydroxide pentahydrate in 100 ml of ethanol solution, and then adding 9.8 g (100 mmol) of methanesulfonic acid. Heat and stir until the generated solid is completely dissolved. Filter the solution and slowly evaporate the solvent at a constant temperature of 30 °C. After several days, transparent crystals will precipitate. To get the crystal of $[NMe_4][CF_3SO_3H]$ ($CF\text{-}NMe_4$), 100 millimoles of tetramethylammonium hydroxide pentahydrate is dissolved in 100 mL of ethanol. Then 100 millimoles of trifluoromethanesulfonic acid was added. Heating and stirring make the solid dissolve, then filter the solution. After the evaporation filter at a constant temperature of 30 °C in the air for several days, plate colorless crystals are obtained. The picture of the crystal is shown in Fig. S1.

Methods

Single-crystal X-ray diffraction (SCXRD): Variable-temperature single-crystal diffraction data were collected on a Rigaku XtaLAB Synergy-S diffractometer (Mo-Kα radiation, λ = 0.71073 Å) equipped with a low-temperature device. A freshly precipitated high-quality single crystal was mounted on a nylon loop under inert oil for analysis. The structure was solved by direct methods using SHELXT-2018 and refined anisotropically for all non-hydrogen atoms via full-matrix least-squares iterations in SHELXL-2018. Hydrogen atoms were geometrically positioned using AFIX instructions and refined isotropically with riding models. CCDC 2449758-2449759 contains the supplementary crystallographic data for this paper. These data can be obtained free of charge via www.ccdc.cam.ac.uk/data_request/cif, by emailing data_request@ccdc.cam.ac.uk.

Powder X-ray diffraction: Temperature-dependent PXRD patterns were recorded on a Rigaku SmartLab SE diffractometer (Mo-Kα radiation, λ = 0.71073 Å). Scans were performed in the 2θ range of 5°–40° (step size 0.02°, scan rate 2° min^{-1}) under a dynamic nitrogen atmosphere. Rietveld refinement was executed using the GSAS-II software suite.

Thermal analysis: Differential scanning calorimetry (DSC) was conducted on a PerkinElmer Diamond DSC instrument. Powdered samples (5.0 ± 0.2 mg) underwent three heating-cooling cycles (20 K/min, N_2 flow 50 mL/min) to ensure reproducibility. Thermogravimetric analysis (TGA) utilized the TA Q50 system system (20 K/min, 300–950 K, N_2 atmosphere), with α-Al_2O_3 as a reference standard.

Second harmonic generation (SHG): SHG measurements were performed using an Edinburgh Instruments FLS 920 fluorescence spectrometer system coupled with a collimated pulsed laser source. The laser source adopted was a Vibrant 355 II laser generator (OPOTEK) excited by pulsed Nd:YAG at a wavelength of 1064 nm, 5 ns pulse duration, 1.6 MW peak power, and a 10 Hz repetition rate.

Dielectric constant measurement: For the dielectric measurements, the polycrystalline samples were ground into powder and pressed into a sheet of about 0.6 mm in thickness, and then the silver glue was evenly spaced on both sides, covering an area of about 15 mm^2. Then copper wire and IC six-hole socket were used to make a capacitor. The Tong hui TH2828A instrument was used to measure the compound dielectric constant ε ($\varepsilon = \varepsilon' - i\,\varepsilon''$).

Hirshfeld surface analysis: The Hirshfeld surfaces and their associated 2D-fingerprint plots were conducted using the Crystal Explorer software, utilizing CIF format structure files as input. The morphology of these surfaces is contingent on the interactions both between molecules within the crystal and between atoms within the molecule. All Hirshfeld surfaces were generated at a standard high surface resolution. The intensity of molecular interactions is visually represented on the Hirshfeld surface through a color scheme comprising red, blue, and white regions. Specifically, white regions correspond precisely to van der Waals contact distances, blue regions indicate longer contacts and red regions signify closer contacts.

The normalized contact distance, denoted as d_{norm}, is derived from the parameters de, di, and the van der Waals (vdW) radii of the two atoms, one external (r_e^{vdW}) and one internal (r_i^{vdW}) to the surface. Mathematically, d_{norm} is defined as:

$$\mathrm{d_{norm}} = \frac{d_i - r^{vdW}}{r_i^{vdW}} + \frac{d_e - r}{r_e^{vdW}}$$

The d_{norm} value is a valuable metric for identifying close intermolecular interactions. A smaller d_{norm} value indicates stronger intermolecular interactions within the system.

Ferroelastic measurement and spontaneous strain tensor calculation: The evolution of domain structures was observed by using an Olympus BX51TRF polarizing microscope at different temperatures controlled by INSTEC HCC602 cooling/heating device. The calculation particular matrix is as follows:

$$\varepsilon_{\mathrm{ij}} = \left[\begin{matrix} \frac{a_{RTP}}{a_{HTP}}\sin\gamma_{RTP} - 1 & \frac{1}{2}\left(\frac{a_{RTP}}{a_{HTP}}\cos\gamma_{RTP}\right) & \frac{1}{2}\bigg(\frac{a_{RTP}\sin\gamma_{RTP}\cos\beta_{HTP}}{a_{HTP}\sin\beta_{HTP}} - \frac{c_{RTP}\sin}{c_{HT}} \\ \frac{1}{2}\left(\frac{a_{RTP}}{a_{HTP}}\cos\gamma_{RTP}\right) & \frac{b_{RTP}}{b_{HTP}} - 1 & \frac{1}{2}\bigg(\frac{c_{RTP}\cos\alpha_{RTP}}{c_{HTP}\sin\beta_{HTP}} + \frac{a_{RTP}\cos\beta_{H}}{a_{HTP}\sin} \\ \frac{1}{2}\left(\frac{a_{RTP}\sin\gamma_{RTP}\cos\beta_{HTP}}{a_{HTP}\sin\beta_{HTP}} - \frac{c_{RTP}\sin\alpha_{RTP}\cos\beta_{RTP}}{c_{HTP}\sin\beta_{HTP}}\right) & \frac{1}{2}\left(\frac{c_{RTP}\cos\alpha_{RTP}}{c_{HTP}\sin\beta_{HTP}} + \frac{a_{RTP}\cos\beta_{HTP}\cos\gamma_{RTP}}{a_{HTP}\sin\beta_{HTP}}\right) & \frac{c_{RTP}\sin\alpha_{RTP}\sin\beta_{RTP}}{c_{HTP}\sin\beta_{HTP}} \end{matrix}\right.$$

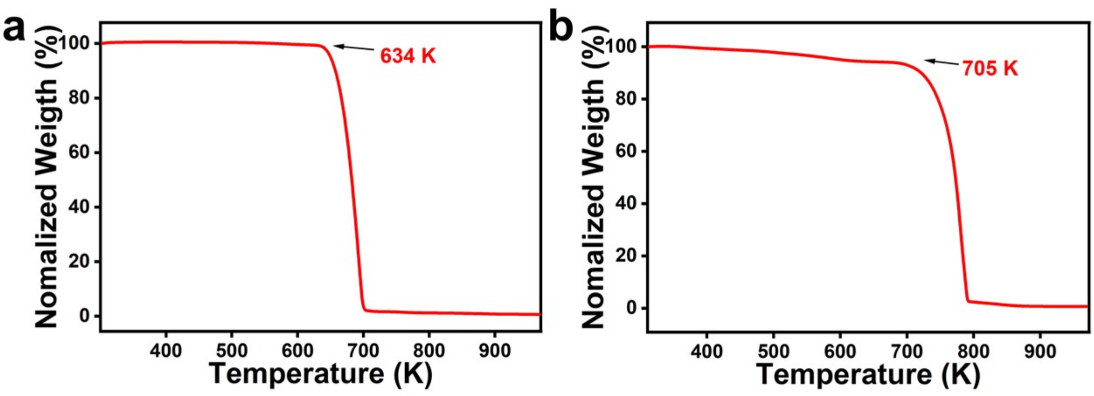

Fig. S1. TGA curves of (a) CH-NMe$_4$, (b) CF-NMe$_4$.

Fig. S2. Piezoelectric coefficient of CH-NMe_4 measured via the quasi-static method..

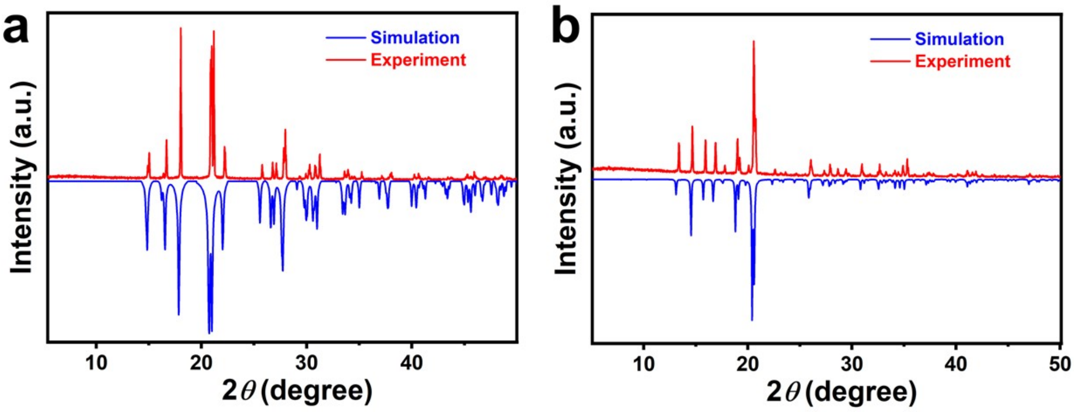

Fig. S3. Simulated and experimental PXRD patterns of (a) CH-NMe_4 at 293 K and (b) CF-NMe_4 at 260 K.

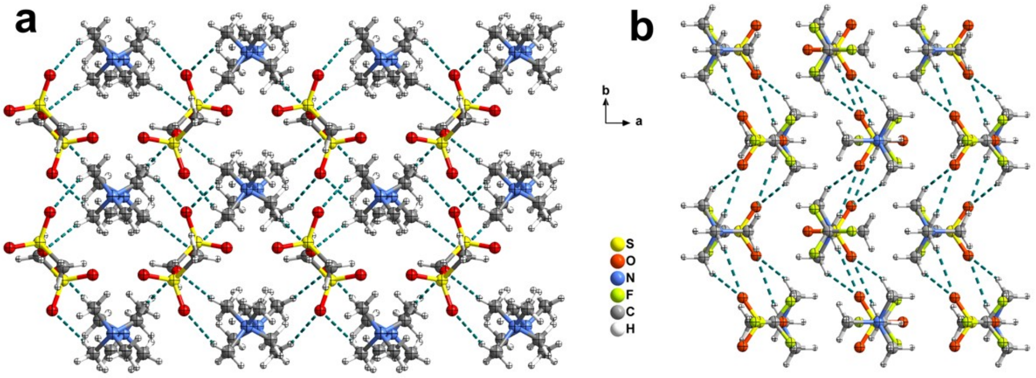

Fig. S4. Two-dimensional tightly connected packing structures of (a) CH-NMe_4 at 293 K, (b) CF-NMe_4 at 260 K from c axis.

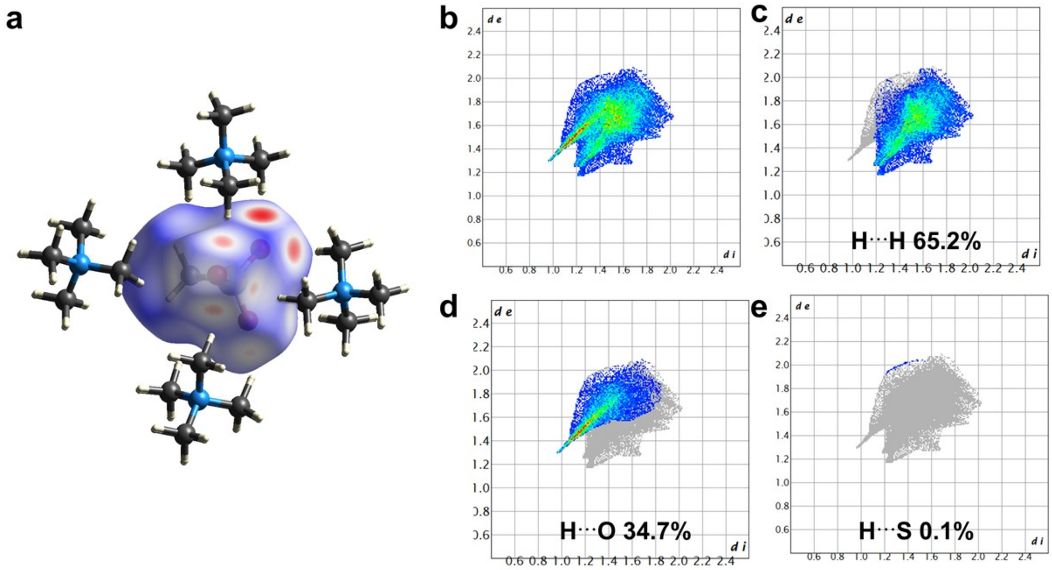

Fig. S5. Visualization map of the distribution of the interactions and the two-dimensional fingerprint plots of CH-NMe$_4$.

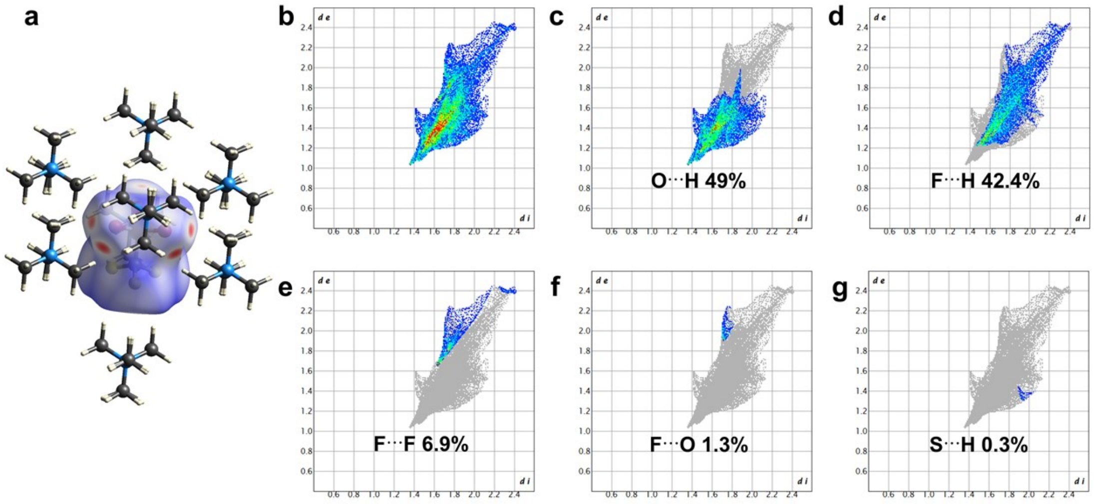

Fig. S6. Visualization map of the distribution of the interactions and the two-dimensional fingerprint plots of CF-NMe.

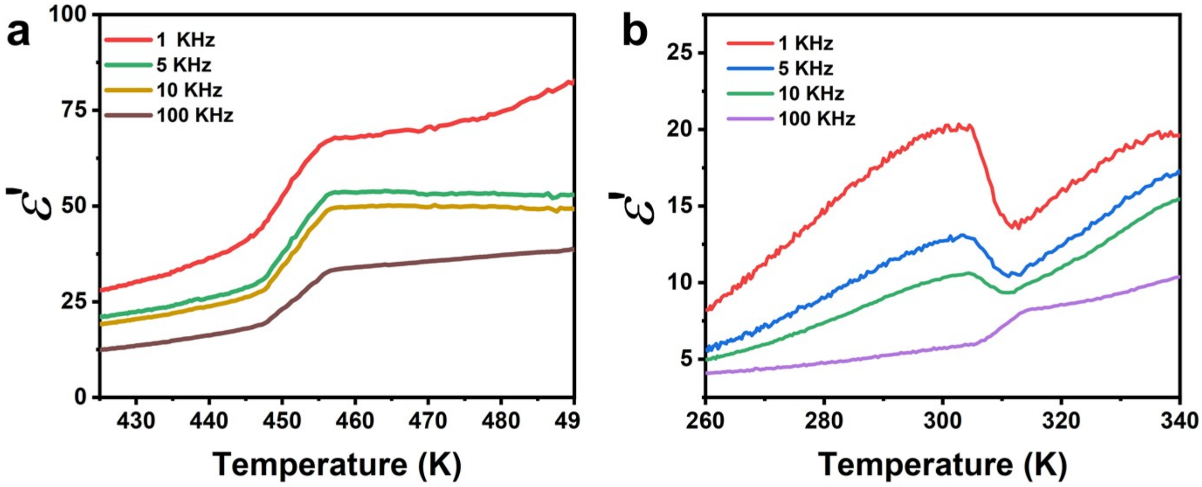

Fig. S7. Temperature-dependent dielectric constants were measured at 1, 5, 10, and 100 kHz for the (a) CH-NMe_4 and (b) CF-NMe_4.

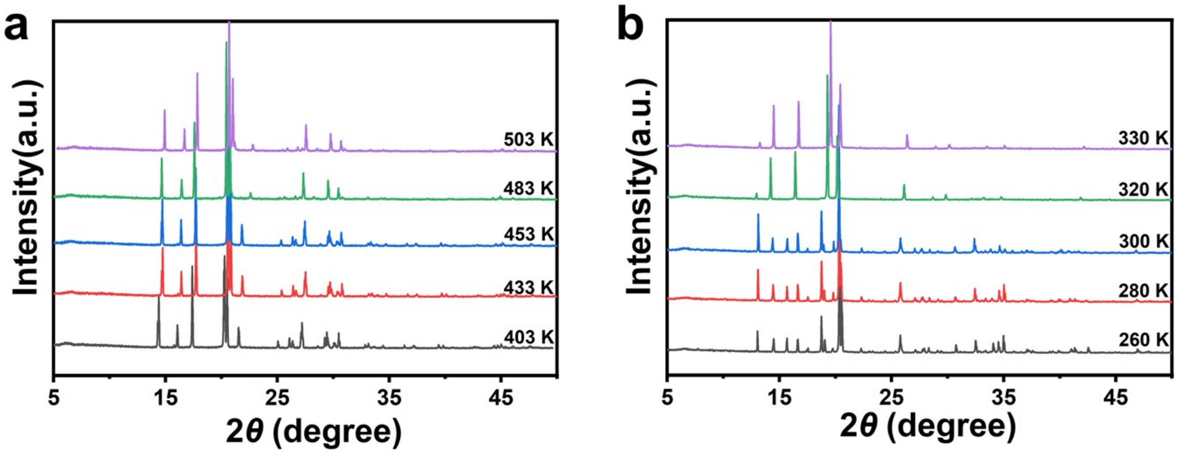

Fig. S8. Variable-temperature PXRD patterns of (a) CH-NMe_4, (b) CF-NMe_4.

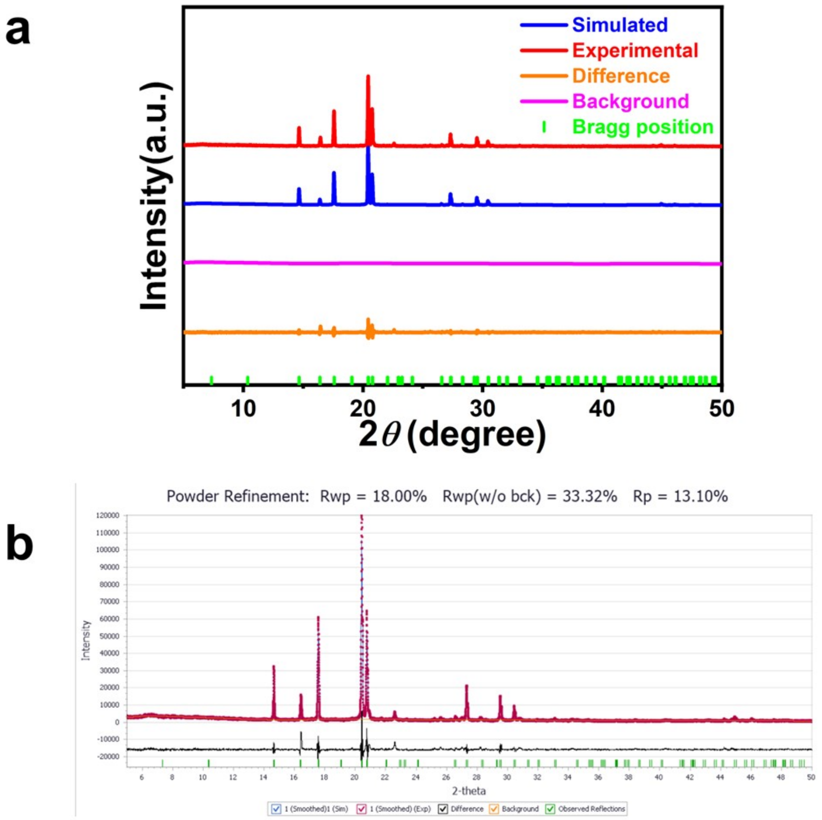

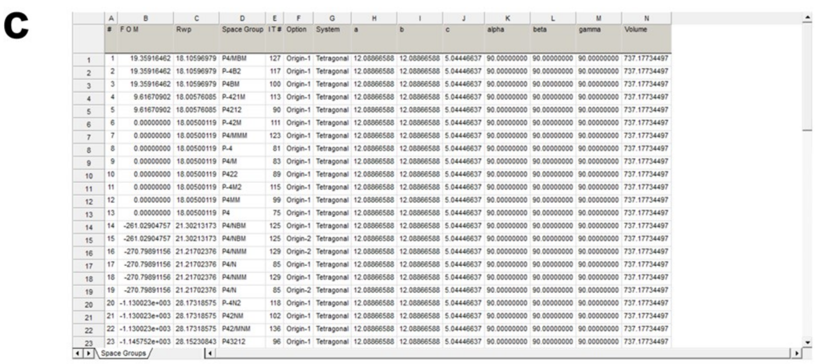

	A	B	C	D	E	F	G	H	I	J	K	L	M	N
	#	F O M	Rwp	Space Group	I T #	Option	System	a	b	c	alpha	beta	gamma	Volume
1	1	19.35916462	18.10596979	P4/MBM	127	Origin-1	Tetragonal	12.08866588	12.08866588	5.04446637	90.00000000	90.00000000	90.00000000	737.17734497
2	2	19.35916462	18.10596979	P-4B2	117	Origin-1	Tetragonal	12.08866588	12.08866588	5.04446637	90.00000000	90.00000000	90.00000000	737.17734497
3	3	19.35916462	18.10596979	P4BM	100	Origin-1	Tetragonal	12.08866588	12.08866588	5.04446637	90.00000000	90.00000000	90.00000000	737.17734497
4	4	9.61670902	18.00576085	P-421M	113	Origin-1	Tetragonal	12.08866588	12.08866588	5.04446637	90.00000000	90.00000000	90.00000000	737.17734497
5	5	9.61670902	18.00576085	P4212	90	Origin-1	Tetragonal	12.08866588	12.08866588	5.04446637	90.00000000	90.00000000	90.00000000	737.17734497
6	6	0.00000000	18.00500119	P-42M	111	Origin-1	Tetragonal	12.08866588	12.08866588	5.04446637	90.00000000	90.00000000	90.00000000	737.17734497
7	7	0.00000000	18.00500119	P4/MMM	123	Origin-1	Tetragonal	12.08866588	12.08866588	5.04446637	90.00000000	90.00000000	90.00000000	737.17734497
8	8	0.00000000	18.00500119	P-4	81	Origin-1	Tetragonal	12.08866588	12.08866588	5.04446637	90.00000000	90.00000000	90.00000000	737.17734497
9	9	0.00000000	18.00500119	P4/M	83	Origin-1	Tetragonal	12.08866588	12.08866588	5.04446637	90.00000000	90.00000000	90.00000000	737.17734497
10	10	0.00000000	18.00500119	P422	89	Origin-1	Tetragonal	12.08866588	12.08866588	5.04446637	90.00000000	90.00000000	90.00000000	737.17734497
11	11	0.00000000	18.00500119	P-4M2	115	Origin-1	Tetragonal	12.08866588	12.08866588	5.04446637	90.00000000	90.00000000	90.00000000	737.17734497
12	12	0.00000000	18.00500119	P4MM	99	Origin-1	Tetragonal	12.08866588	12.08866588	5.04446637	90.00000000	90.00000000	90.00000000	737.17734497
13	13	0.00000000	18.00500119	P4	75	Origin-1	Tetragonal	12.08866588	12.08866588	5.04446637	90.00000000	90.00000000	90.00000000	737.17734497
14	14	-261.02904757	21.30213173	P4/NBM	125	Origin-1	Tetragonal	12.08866588	12.08866588	5.04446637	90.00000000	90.00000000	90.00000000	737.17734497
15	15	-261.02904757	21.30213173	P4/NBM	125	Origin-2	Tetragonal	12.08866588	12.08866588	5.04446637	90.00000000	90.00000000	90.00000000	737.17734497
16	16	-270.79891156	21.21702376	P4/NMM	129	Origin-2	Tetragonal	12.08866588	12.08866588	5.04446637	90.00000000	90.00000000	90.00000000	737.17734497
17	17	-270.79891156	21.21702376	P4/N	85	Origin-1	Tetragonal	12.08866588	12.08866588	5.04446637	90.00000000	90.00000000	90.00000000	737.17734497
18	18	-270.79891156	21.21702376	P4/NMM	129	Origin-1	Tetragonal	12.08866588	12.08866588	5.04446637	90.00000000	90.00000000	90.00000000	737.17734497
19	19	-270.79891156	21.21702376	P4/N	85	Origin-2	Tetragonal	12.08866588	12.08866588	5.04446637	90.00000000	90.00000000	90.00000000	737.17734497
20	20	-1.130023e+003	28.17318575	P-4N2	118	Origin-1	Tetragonal	12.08866588	12.08866588	5.04446637	90.00000000	90.00000000	90.00000000	737.17734497
21	21	-1.130023e+003	28.17318575	P42NM	102	Origin-1	Tetragonal	12.08866588	12.08866588	5.04446637	90.00000000	90.00000000	90.00000000	737.17734497
22	22	-1.130023e+003	28.17318575	P42/MNM	136	Origin-1	Tetragonal	12.08866588	12.08866588	5.04446637	90.00000000	90.00000000	90.00000000	737.17734497
23	23	-1.145752e+003	28.15230843	P43212	96	Origin-1	Tetragonal	12.08866588	12.08866588	5.04446637	90.00000000	90.00000000	90.00000000	737.17734497

Fig. S9. The final Rietveld refinement plot of CH-NMe$_4$ structure at 330 K in the high-temperature phase: experimental pattern (red line), calculated pattern (blue line), difference profile (yellow line), background (pink line), and background profile (green dot). Through the Rietveld refinements of the PXRD data, we obtained the tetragonal crystal system, among which the most possible point group is 4/*m*.

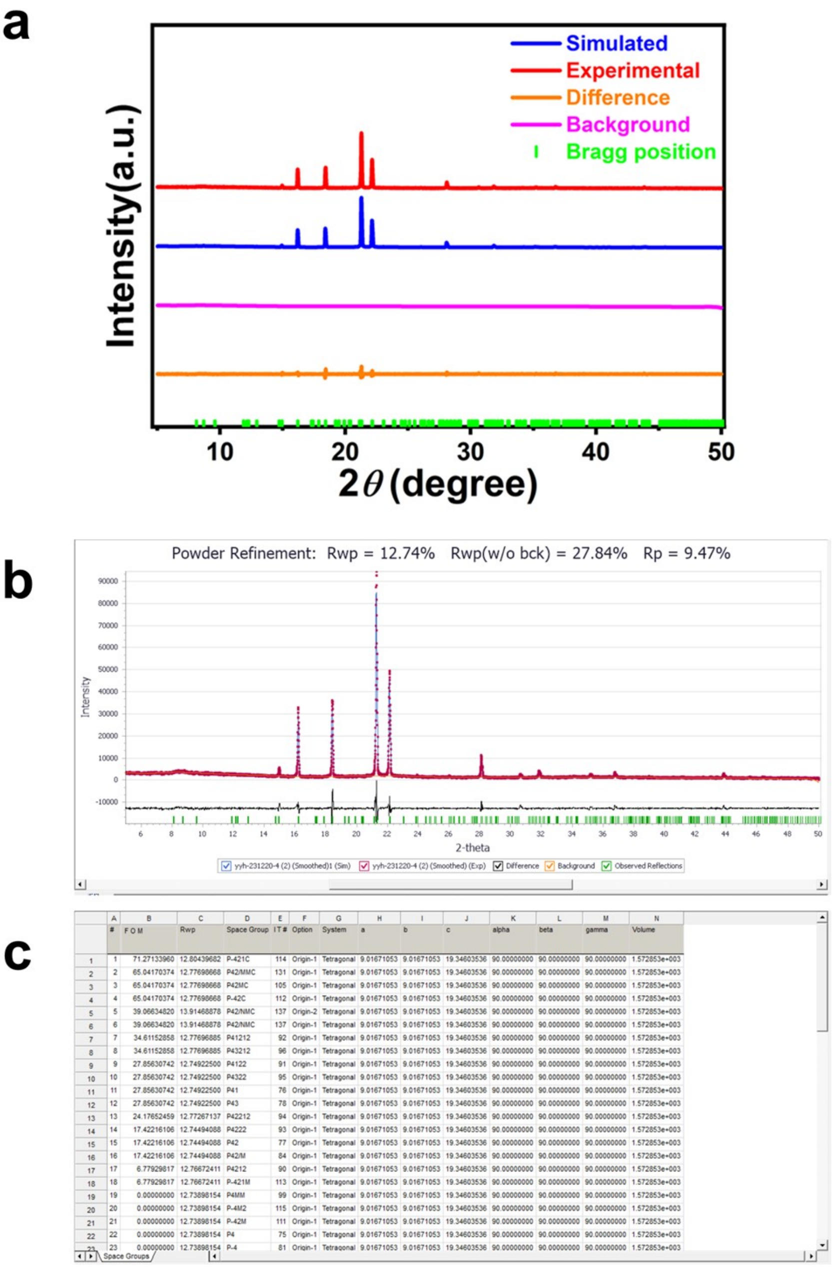

	A	B	C	D	E	F	G	H	I	J	K	L	M	N
	#	F O M	Rwp	Space Group	I T #	Option	System	a	b	c	alpha	beta	gamma	Volume
1	1	71.27133960	12.80439682	P-421C	114	Origin-1	Tetragonal	9.01671053	9.01671053	19.34603536	90.00000000	90.00000000	90.00000000	1.572853e+003
2	2	65.04170374	12.77698668	P42/MMC	131	Origin-1	Tetragonal	9.01671053	9.01671053	19.34603536	90.00000000	90.00000000	90.00000000	1.572853e+003
3	3	65.04170374	12.77698668	P42MC	105	Origin-1	Tetragonal	9.01671053	9.01671053	19.34603536	90.00000000	90.00000000	90.00000000	1.572853e+003
4	4	65.04170374	12.77698668	P-42C	112	Origin-1	Tetragonal	9.01671053	9.01671053	19.34603536	90.00000000	90.00000000	90.00000000	1.572853e+003
5	5	39.06634820	13.91468878	P42/NMC	137	Origin-2	Tetragonal	9.01671053	9.01671053	19.34603536	90.00000000	90.00000000	90.00000000	1.572853e+003
6	6	39.06634820	13.91468878	P42/NMC	137	Origin-1	Tetragonal	9.01671053	9.01671053	19.34603536	90.00000000	90.00000000	90.00000000	1.572853e+003
7	7	34.61152858	12.77696885	P41212	92	Origin-1	Tetragonal	9.01671053	9.01671053	19.34603536	90.00000000	90.00000000	90.00000000	1.572853e+003
8	8	34.61152858	12.77696885	P43212	96	Origin-1	Tetragonal	9.01671053	9.01671053	19.34603536	90.00000000	90.00000000	90.00000000	1.572853e+003
9	9	27.85630742	12.74922500	P4122	91	Origin-1	Tetragonal	9.01671053	9.01671053	19.34603536	90.00000000	90.00000000	90.00000000	1.572853e+003
10	10	27.85630742	12.74922500	P4322	95	Origin-1	Tetragonal	9.01671053	9.01671053	19.34603536	90.00000000	90.00000000	90.00000000	1.572853e+003
11	11	27.85630742	12.74922500	P41	76	Origin-1	Tetragonal	9.01671053	9.01671053	19.34603536	90.00000000	90.00000000	90.00000000	1.572853e+003
12	12	27.85630742	12.74922500	P43	78	Origin-1	Tetragonal	9.01671053	9.01671053	19.34603536	90.00000000	90.00000000	90.00000000	1.572853e+003
13	13	24.17652459	12.77267137	P42212	94	Origin-1	Tetragonal	9.01671053	9.01671053	19.34603536	90.00000000	90.00000000	90.00000000	1.572853e+003
14	14	17.42216106	12.74494088	P4222	93	Origin-1	Tetragonal	9.01671053	9.01671053	19.34603536	90.00000000	90.00000000	90.00000000	1.572853e+003
15	15	17.42216106	12.74494088	P42	77	Origin-1	Tetragonal	9.01671053	9.01671053	19.34603536	90.00000000	90.00000000	90.00000000	1.572853e+003
16	16	17.42216106	12.74494088	P42/M	84	Origin-1	Tetragonal	9.01671053	9.01671053	19.34603536	90.00000000	90.00000000	90.00000000	1.572853e+003
17	17	6.77929817	12.76672411	P4212	90	Origin-1	Tetragonal	9.01671053	9.01671053	19.34603536	90.00000000	90.00000000	90.00000000	1.572853e+003
18	18	6.77929817	12.76672411	P-421M	113	Origin-1	Tetragonal	9.01671053	9.01671053	19.34603536	90.00000000	90.00000000	90.00000000	1.572853e+003
19	19	0.00000000	12.73898154	P4MM	99	Origin-1	Tetragonal	9.01671053	9.01671053	19.34603536	90.00000000	90.00000000	90.00000000	1.572853e+003
20	20	0.00000000	12.73898154	P-4M2	115	Origin-1	Tetragonal	9.01671053	9.01671053	19.34603536	90.00000000	90.00000000	90.00000000	1.572853e+003
21	21	0.00000000	12.73898154	P-42M	111	Origin-1	Tetragonal	9.01671053	9.01671053	19.34603536	90.00000000	90.00000000	90.00000000	1.572853e+003
22	22	0.00000000	12.73898154	P4	75	Origin-1	Tetragonal	9.01671053	9.01671053	19.34603536	90.00000000	90.00000000	90.00000000	1.572853e+003
23	23	0.00000000	12.73898154	P-4	81	Origin-1	Tetragonal	9.01671053	9.01671053	19.34603536	90.00000000	90.00000000	90.00000000	1.572853e+003

Fig. S10. The final Rietveld refinement plot of CF-NMe_4 structure at 503 K in the high-temperature phase: experimental pattern (red line), calculated pattern (blue line), difference profile (yellow line), background (pink line), and background profile (green dot). Through the Rietveld refinements of the PXRD data, we obtained the tetragonal crystal system, among which the most possible point groups are 4/*mmm* and 4/*m*.

Table S1. Variable-temperature crystallographic data of the single-crystal of CH-NMe_4 and CF-NMe_4.

Compound	CH-NMe_4	CF-NMe_4
Temperature/K	293	260
Crystal system	Orthorhombic	Monoclinic
Empirical formula	$C_5H_{15}NO_3S$	$C_5H_{12}F_3NO_3S$
Formula weight	169.24	223.22
Space group	$Pca2_1$	$P2_1/m$
a/Å	11.994(2)	10.3722(3)
b/Å	6.1359(13)	8.6225(2)
c/Å	11.923(3)	11.6086(3)
α/°	90	90
β/°	90	103.824(3)
γ/°	90	90
Volume/Å^3	877.5(3)	1008.13(5)
Z	4	4
Radiation	$MoK\alpha$(λ=0.71073)	$MoK\alpha$(λ=0.71073)
ρ_{calc}g/cm^3	1.281	1.471
GOF	1.040	1.076
Final R indexes [I>=2σ(I)]	R_1=0.0807 wR_2=0.1467	R_1 = 0.0795, wR_2 = 0.2161

Table S2. Non-classical Hydrogen Bonds for CH-NMe_4 at 293 K

D	H	A	d(*D*−H)/Å	d(H−*A*)/Å	d(D−*A*)/Å	*D*−H−A/°
C1	H1C	O2	0.96	2.52	3.457	167
C3	H3B	O1	0.96	2.58	3.511	164
C4	H4B	O2	0.96	2.40	3.349	170
C4	H4C	O1	0.96	2.60	3.539	167

Table S3. Non-classical Hydrogen Bonds for CF-NMe_4 at 260 K

D	H	A	d(*D*−H)/Å	d(H−*A*)/Å	d(D−*A*)/Å	*D*−H−A/°
C2	H2C	O3	0.96	2.56	3.420	149
C3	H3C	O3	0.96	2.50	3.373	151
C5	H5A	O1	0.96	2.56	3.414	148
C5	H5B	O1	0.96	2.53	3.414	153
C6	H6A	O2	0.96	2.57	3.442	151
C6	H6B	O1	0.96	2.56	3.420	150